CHEMISTRY OF MATERIALS
Cite This: Chem. Mater. 2019, 31, 8019–8025
Article
pubs.acs.org/cm

Indium-Free Amorphous Ca–Al–O Thin Film as a Transparent Conducting Oxide

So Hee Sim,[#,†] Kyeong Tae Kang,[#,†] Sangyun Lee,[†] Miso Lee,[‡] Hiroki Taniguchi,[§] Suyoung Kim,[†] Seulki Roh,[†] Jun Hyeob Oh,[∥] Sang A Lee,[†] Jong-Seong Bae,[⊥] Jae Hyuck Jang,[∥] Jungseek Hwang,[†] Seungwu Han,[‡] Tuson Park,[†] and Woo Seok Choi*[,†]

[†]Department of Physics, Sungkyunkwan University, Suwon 16419, Korea
[‡]Department of Materials Science and Engineering, Seoul National University, Seoul 08826, Republic of Korea
[§]Department of Physics, Nagoya University, Nagoya 464-8602, Japan
[∥]Center for Research Equipment, Korea Basic Science Institute, Daejeon 34133, Korea
[⊥]Busan Center, Korea Basic Science Institute, Busan 46742, Korea

Supporting Information

ABSTRACT: Transparent conducting oxide (TCO) is a promising material system for transparent electrodes, which is one of the most essential elements in current electronic and energy devices. In particular, In-based TCOs such as Sn:In_2O_3 (ITO) and In–Ga–Zn–O (IGZO) have shown large optical band gap and high electrical conductivity, sufficient for the applications. However, In is an expensive element, which hampers its facile industrial application. Moreover, In-based TCOs show an abrupt decrease in conductivity when their thickness decreases below ∼100 nm, possibly due to inhomogeneity within the thin films. Here, we introduce an amorphous Ca–Al–O (CAO) thin film as a promising candidate for the In-free TCOs. The amorphous CAO thin film has very low resistivity (∼10^{-5} Ω cm) at room temperature, as well as high transparency in the visible region of the light spectrum (>80%). The isotropic Ca *s*-orbital in the conduction band is found to be responsible for the superior performance of CAO as a TCO. Owing to the exceptional structural homogeneity of the CAO thin film, thickness-independent transport characteristics are observed, maintaining its TCO performance down to 10 nm of thickness.

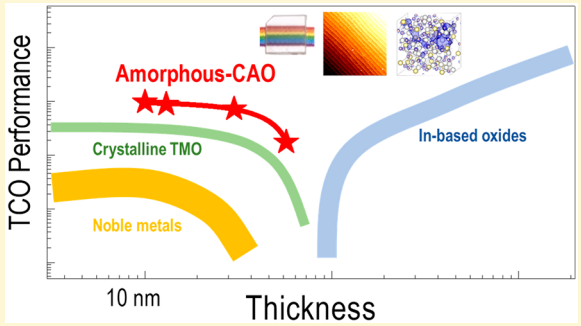

INTRODUCTION

A highly efficient transparent conductor is one of the most essential components in the state-of-the-art optoelectronic and energy applications.[1−3] Working transparent conducting electrodes require the combination of incompatible physical properties, i.e., high transmittance (>80%) in the photon energy range from 1.75 to 3.25 eV, considerably large optical band gap (>3 eV), and low electrical resistivity (<10^{-3} Ω cm) with high carrier concentration (>10^{20} cm^{-3}).[1,4,5] In addition to metallic or carbon-based nanostructured films and nanowires which have been extensively studied,[6−9] some oxide materials, known as transparent conducting oxides (TCOs), show high electrical conductivity while maintaining their transparency.[1,10,11] The concept of heavy doping of light carriers into a wide bandgap material has been largely adopted, represented by Sn-doped In_2O_3 (ITO).[12] Owing to the ionized impurity scattering, ITO and other In-based TCOs exhibit high mobility compared to the noble metals.[1,13] Hosono's group further proposed the amorphous In–Ga–Zn–O, which shows many advantages including flexibility and facility in fabrication, for the display industry.[14−17]

On the other hand, substantial research efforts have been made in the search for In-free TCO materials. First, the next generation of TCOs should be composed of earth-abundant elements. Post-transition metal elements such as In, Sn, and Zn[18] are extensively employed in TCOs. They possess *s*-orbitals with the configuration of $(n-1)d^{10}ns^0$, which is highly beneficial for isotropic electrical conduction.[14,15] However, these elements, especially In, are rather scarce and expensive. Second, In-based films show a dramatic reduction of carrier concentration and mobility as their thicknesses decrease below 100 nm, leading to an abrupt degradation of their TCO figure of merit. While the exact origin of this thickness-dependent degradation is not clear, the structural irregularity or the defect inhomogeneity of crystalline In-based materials might be responsible.[19−23] On the contrary, some In-free TCOs show promising efficiency with the thickness of tens of nanometers.[24,25] For the thin-film transistor applications, TCOs operating in this thin-thickness limit are highly necessary.

Received: June 19, 2019
Revised: September 5, 2019
Published: September 6, 2019

DOI: 10.1021/acs.chemmater.9b02399
Chem. Mater. 2019, 31, 8019–8025

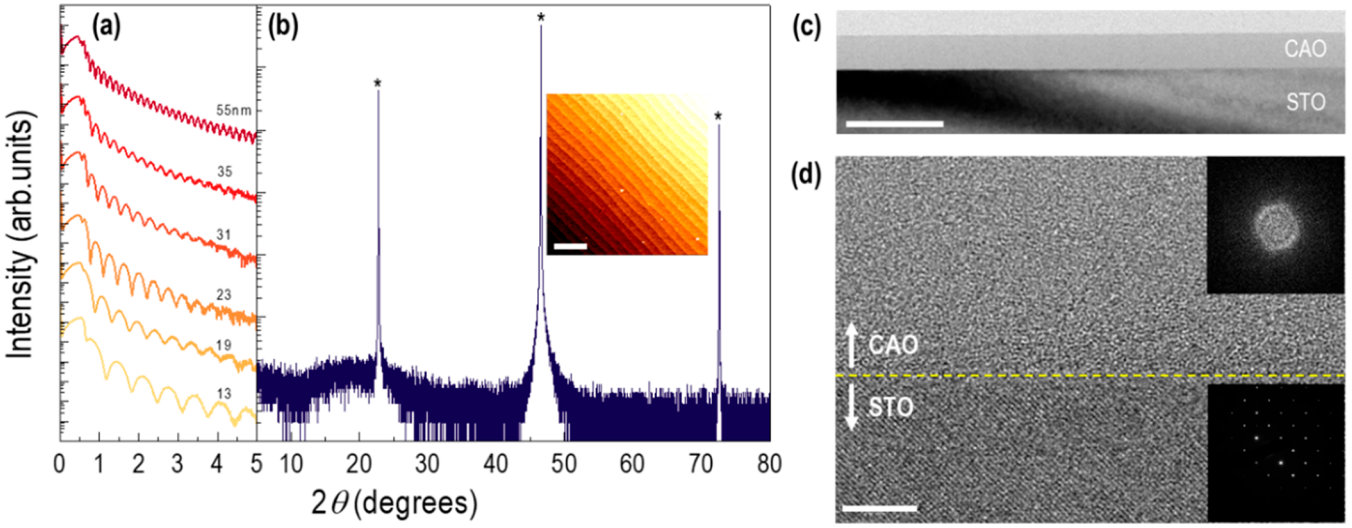

Figure 1. Atomically flat amorphous CAO thin films. (a) The X-ray reflectivity scans of the CAO thin films show clear thickness-fringe patterns. (b) Typical X-ray diffraction $\theta-2\theta$ scan result of an amorphous CAO thin film. Stars (*) denote the (001), (002), and (003) Bragg reflections of the STO substrate. The inset shows an AFM topography image of the CAO thin film, maintaining the step-and-terrace structure of the substrate. The scale bar denotes 1 μm. (c) Low-magnification cross-sectional TEM image of the CAO thin film on an STO substrate. The scale bar denotes 100 nm. (d) High-resolution cross-sectional TEM image of the CAO thin film. The scale bar denotes 5 nm. Top and bottom insets show the FFT images of the amorphous CAO thin film and the crystalline STO substrate, respectively.

In this paper, we propose Ca−Al−O (CAO) as an ultrathin In-free amorphous TCO film, with a competitive figure of merit. In contrast to the conventional TCOs with post-transition metal elements, *s*-orbitals of Ca, an earth-abundant alkaline earth metal, constitute the conduction band and function as the electron pathway in amorphous CAO. By characterizing the optical and electrical properties of the CAO thin films as thin as 9 nm, we confirm that the transparent CAO thin films maintain robust TCO performances irrespective to thickness reduction.

RESULTS AND DISCUSSIONS

Amorphous CAO thin films with atomically flat surfaces have been fabricated using pulsed laser deposition (PLD). Figure 1 shows the structural properties of CAO thin films deposited on single-crystalline $SrTiO_3$ (STO) substrates. A representative X-ray diffraction $\theta-2\theta$ scan (Figure 1b) does not show Bragg diffraction peaks other than those from the substrate. On the other hand, the X-ray reflectivity (XRR) measurement (Figure 1a) presents an apparent fringe pattern, providing the thickness of the thin film and assuring the extremely flat nature of the surface and the interface of the amorphous thin film. The one-unit cell step-and-terrace structure in the topography measured by atomic force microscopy (AFM) further validates the atomically flat surface of the CAO thin films, with very low root-mean-square (RMS) roughness (<1 nm, inset of Figure 1b). In the cross-sectional image obtained by transmission electron microscopy (TEM), the well-defined surface and interface, as well as the highly homogeneous nature of the CAO thin film, is observed (Figure 1c). Employing the TEM−electron dispersive spectroscopy (EDS), we further confirmed the exceptional structural and chemical homogeneity of the CAO thin films (Figure S1a). The high-resolution TEM image in Figure 1d depicts the atomically flat interface between the amorphous CAO thin film and STO substrate. The fast Fourier transformation (FFT) image of the CAO thin film (upper inset) shows hazy rings that indicate the amorphous nature of the thin film.

The amorphous CAO thin film has a sizable optical band gap, giving rise to high transparency. We measured the optical transmittance spectra (Tr) of the CAO thin films in the photon energy range of 0.62−6.2 eV, as shown in Figure 2a. In the visible range, Tr decreases systematically with the increase of the film thickness. The photographic images shown in the inset of Figure 2b provide the clear transparent nature of the thin films in the visible range. In the low photon energy range, the Drude absorption is evidenced, indicating that the CAO thin films are conducting.[24,26−28] We additionally performed optical transmittance simulation based on the metallic CAO thin film, which reproduces the transmittance spectral features obtained experimentally (see Figure S2 and Supporting Information for detail). The optical band gap of the CAO thin film is larger than that of the STO substrate, i.e., 3.2 eV, and Tr above 3.2 eV is limited by the substrate. Note that the larger Tr of the thin films around 3.0 eV, compared to the STO substrate, is due to the antireflection effect. We further extracted the Tr spectra of the CAO thin films without the substrate by deducing the optical dielectric functions of CAO satisfying the Tr results (see Supporting Information for detail). Figure 2b shows that the CAO thin films have high Tr, with the thinnest sample showing almost 95% of Tr in the visible range, manifesting superior optical properties of the CAO thin films.

The amorphous CAO thin films show good electrical conductivity at room temperature. Figure 2c,d shows the sheet resistance (R_s) and the sheet carrier concentration (n_s) of the CAO thin films as a function of temperature, respectively. R_s decreases largely (3 orders of magnitude) with the decreasing temperature, indicating a robust metallic behavior. The resistivity (ρ) and the bulk carrier concentration (n) of the CAO thin films are shown in Figures 2e,f, respectively. Despite their amorphous nature, the CAO thin films show very low ρ ($\sim 10^{-5}$ Ω cm) with high n ($\sim 10^{22}$ cm^{-3}) at room temperature when compared to other TCOs with thicknesses of tens of nanometers. If the metallic conduction were to originate from the film/surface interface and not from the CAO thin film, a

DOI: 10.1021/acs.chemmater.9b02399
Chem. Mater. 2019, 31, 8019−8025

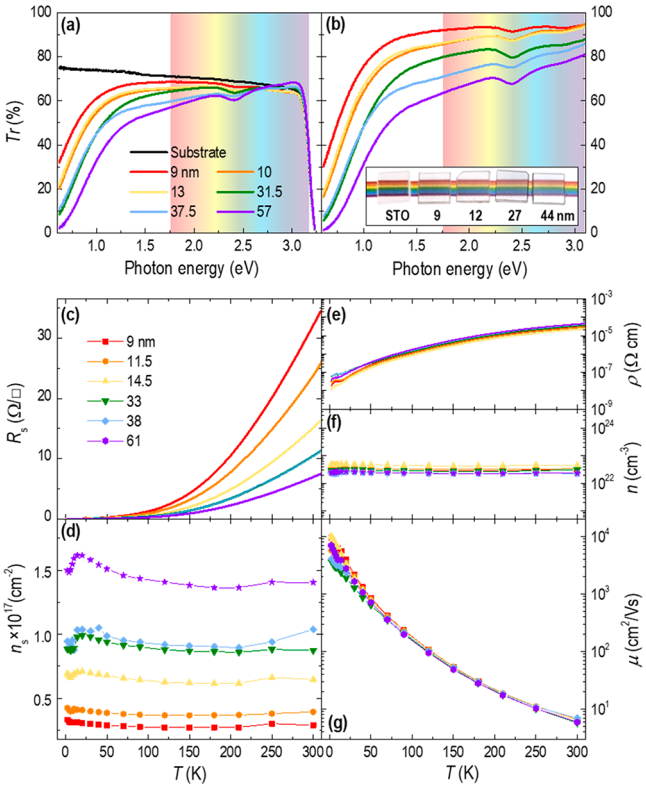

Figure 2. Optical and electrical properties of the CAO thin films. (a) Transmittance spectra of the CAO thin films with various thicknesses deposited on top of the STO substrates. The STO substrate (black line) was annealed at the growth condition for 1 h for comparison. (b) Transmittance spectra only for the CAO thin films. The inset shows photographic images of the CAO thin films with various thicknesses. Temperature-dependent (c) sheet resistance and (d) sheet carrier concentration of CAO thin films. Temperature-dependent (e) resistivity, (f) carrier concentration, and (g) mobility of the CAO thin films showing a linear scaling with the thickness.

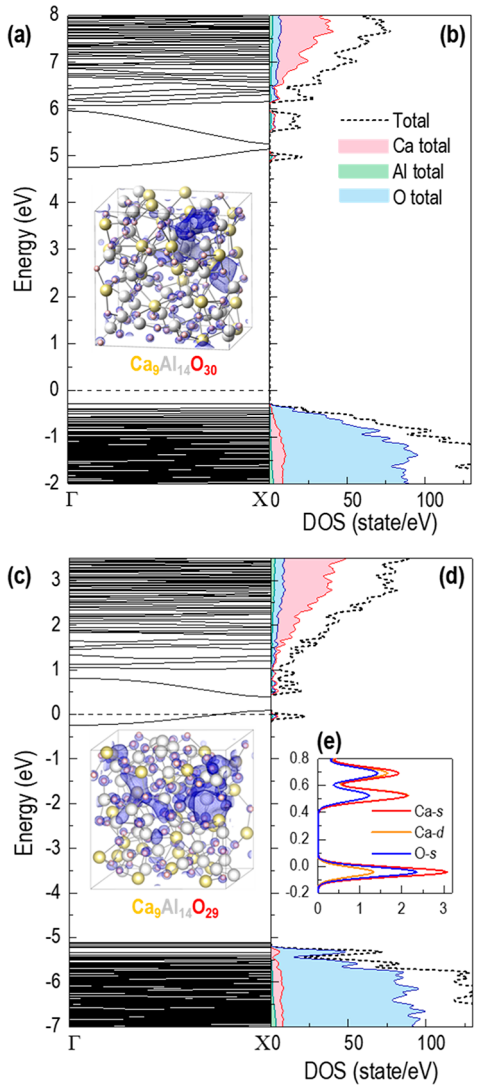

Figure 3. First-principles calculation results. (a) Energy band dispersion of $Ca_9Al_{14}O_{30}$, showing the Fermi level near the valence band maximum. (b) Projected density of states for $Ca_9Al_{14}O_{30}$. (c) Energy band dispersion of $Ca_9Al_{14}O_{29}$ with the oxygen vacancies introduced, leading to an increase in the Fermi level. The insets in (a) and (c) illustrate the charge density of Ca dominated by the *s*-orbital (blue color) at the Γ points. (d) Projected density of states for $Ca_9Al_{14}O_{29}$. (e) Enlarged density of states of Ca and O orbitals around the Fermi level.

constant R_s value is predicted independent of the film thickness. Therefore, the exact linear scaling of ρ and n with respect to the thickness of the thin film, i.e., the CAO thin films show the same ρ and n value independent of the thickness, confirms that the CAO thin film is indeed metallic.

The theoretical calculation provided the origin of the large optical band gap of the CAO thin films. We used molecular dynamics (MD) calculations to estimate the band structure of the amorphous CAO. The chemical composition of the thin film was first estimated experimentally using X-ray photoelectron spectroscopy (XPS), providing atomic concentration ratios of 9.1 ± 0.5 and 14.2 ± 0.5 for Ca and Al, respectively (see Figure S3b,c and Supporting Information for detail). As the oxygen concentration is rather difficult to determine experimentally in the presence of the oxide substrate, we first fixed the cation ratio as 9/14 for Ca/Al for the MD calculation. Then, several oxygen concentrations within the thin film were estimated to reproduce the experimental results (see Supporting Information for detail). The MD results of a stoichiometric $Ca_9Al_{14}O_{30}$ structure (CAO_{30}) and an oxygen deficient $Ca_9Al_{14}O_{29}$ structure (CAO_{29}) are shown in Figure 3a,c, respectively. The stoichiometric CAO_{30} shows an insulating band structure with a large band gap (>5 eV). By slightly doping the oxygen vacancy (CAO_{29}), the Fermi level near the valence band maximum moves toward the conduction band minimum, owing to the induced free charge carriers. A Burstein−Moss shift can be anticipated, leading to an n-type carrier with a wide optical band gap. It is noteworthy that the MD calculation results manifest the importance of the oxygen stoichiometry in determining the intrinsic transport properties of the CAO thin film. Indeed, the desired transport properties can only be realized by achieving a precise stoichiometry. With the correct stoichiometry, the result of the MD calculation of CAO_{29} is consistent with the experimentally observed transport behavior (Figure 2). When more oxygen vacancies are introduced to the system, Al clusters are generated leading to midgap defect states (Figure S4), leading to an opaque material.

Figure 3b,d shows the projected density of states (DOS) of CAO_{30} and CAO_{29}, respectively. The conduction bands are mainly comprised of strongly hybridized orbital states of Ca

DOI: 10.1021/acs.chemmater.9b02399
Chem. Mater. 2019, 31, 8019−8025

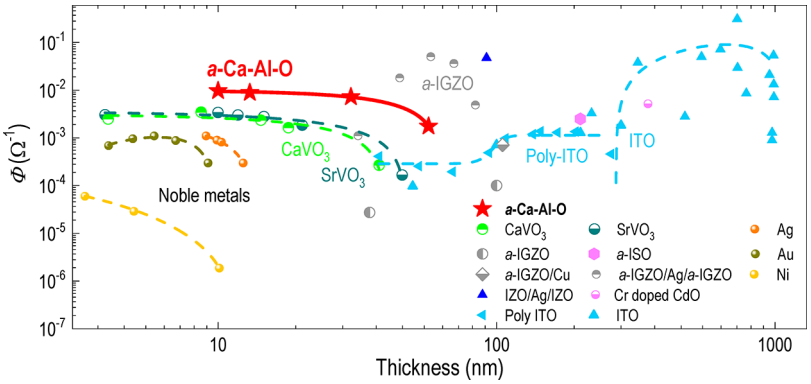

Figure 4. Thickness-dependent Haacke figure of merit of the TCO thin films. For comparison, the figure of merit values of the state-of-the-art transparent conducting materials are also shown with the trend lines. The CAO thin film shows a superior figure of merit in the thin-thickness region.

and O. In particular, the states around the Fermi level for the CAO_{29}, giving rise to the electrical conduction, are mainly Ca *s* orbital states, as depicted in Figure 3e. The insets in Figure 3a,c illustrate the charge density obtained through the MD calculations, in which the Ca *s* orbital is expressed in blue. Indeed, CAO_{29} shows widely spread orbitals of the Ca 4*s*, in part by hybridization with oxygen ions predominantly in the conduction band. This overlap of the orbitals can be considered as the origin of the high conductivity of the amorphous CAO thin films. The band dispersion of CAO_{29} also provides an estimation of the effective mass, which further justifies the transparent nature of the amorphous CAO thin films. Herein, the flat band dispersion leads to a rather large effective mass of $m^* = \sim 5\ m_e$. Regarding the plasma frequency, $\omega_p = [ne^2/m^*\varepsilon_0]^{1/2}$, where e is the electronic charge and ε_0 is the permittivity of free space, a large m^* corresponds to a small ω_p, allowing high transparency in the visible wavelength of light.

We note that the highly metallic behavior of the CAO thin films was not achieved on other substrates including $LaAlO_3$, LSAT, and SiO_2/Si, with limited trials. This would lead to a possibility that the STO substrates might have become conducting as they have become reduced during the growth. The temperature-dependent electronic transport behavior of the CAO/STO system resembles that of the STO, partially supporting this possibility. However, as shown previously, the metallic behavior of the CAO thin films was confirmed by the MD calculations to be intrinsic. This indicates that a specific type of substrate (STO in this case) might have promoted the right stoichiometry of the CAO thin film, as the metallic behavior is highly susceptible to the chemical stoichiometry. In addition, we present further experimental evidence that the conductivity of the CAO/STO samples is indeed originating from the CAO thin films and the STO substrate is insulating.

To confirm the insulating phase of the STO substrate, we first employed scanning transmission electron microscopy–electron energy loss spectroscopy (STEM-EELS) (Figure S1b). If a sufficient amount of oxygen vacancies is introduced in STO to induce the metallic behavior, the crystal field splitting of the Ti *d*-orbitals (Δ) becomes largely suppressed.[29] This can be directly observed from the decrease in Δ value between the t_{2g} and e_g peaks of the Ti L_2 and L_3-edge, i.e., the nominal value of Δ = 2.2–2.3 eV of the stoichiometric STO decreases to 1.8–1.9 eV for the reduced STO. The first peak of the O *K*-edge also shows smearing as oxygen vacancies are introduced. These signatures of oxygen vacancies in STO are not observed in our STEM-EELS measurements as shown in Figure S1. Even at the very interface with the CAO, the electronic structure of STO remains highly insulating without any signature of oxygen vacancies. Second, the STO substrate remains robustly insulating and transparent (black line in Figure 2a) even after annealing at the CAO thin film growth conditions (1 h in 700 °C with oxygen partial pressure of 10^{-5} Torr). It is indeed possible that the PLD growth could introduce oxygen vacancies in the STO substrate when the growth occurs at a low oxygen partial pressure. However, more recent studies show that the plume dynamics is the deterministic factor and not the oxygen partial pressure for the creation of oxygen vacancies. For example, using a weak laser plume, one can *deposit* insulating STO thin film on STO substrate even in the high vacuum of 10^{-6} Torr with a laser fluence of 1 J cm^{-2}.[30] In our case, we use higher oxygen partial pressure of 10^{-5} Torr and the lower laser fluence of 0.76 J cm^{-2} for CAO thin film growth. In such a case, it is not plausible to introduce an oxygen vacancy during the growth. Third, both $\rho(T)$ and n are almost perfectly scaled with respect to the thickness of the CAO thin films (see Figure 2e,f). The exact same argument has been proposed to argue that the STO substrate is insulating even underneath the $LaTiO_3$ thin film, which is known to induce a large charge transfer via electrostatic potential mismatch.[31] Finally, the optical signature also argues strongly against the formation of oxygen vacancies in STO. When oxygen vacancies are introduced in STO, it is well-known that a strong, characteristic optical absorption always occurs at ~1.5 eV due to the formation of the in-gap state.[32−34] This absorption or any other defect state related absorption were not observed in our CAO/STO thin film, consistent with the metallic behavior of CAO obtained by the theoretical calculation. We note that additional studies might be required to investigate the metallic behavior in further detail, but our experimental and theoretical results consistently point toward the intrinsic metallic behavior of the CAO thin films.

By summarizing the optical and electrical properties, the CAO thin films exhibit a superior TCO performance, especially in the thin-thickness limit. Figure 4 summarizes the Haacke figure of merit of TCO performance, i.e., $\Phi = Tr^{10}/R_s$.[35] The room-temperature values of Φ of the CAO thin films are shown along with other state-of-the-art transparent conductors, e.g., $(Ca,Sr)VO_3$,[24] Cr-doped CdO,[36] amorphous

DOI: 10.1021/acs.chemmater.9b02399
Chem. Mater. 2019, 31, 8019−8025

(*a*-)IGZO,[21,37,38] *a*-IGZO/Cu,[37] *a*-IGZO/Ag/*a*-IGZO,[39] *a*-ISO,[40] IZO/Ag/IZO,[41] poly-ITO,[1] ITO,[1,24,35,42] Ag,[43] Au,[24] and Ni.[44] By plotting Φ as a function of the film thickness, it is evident that the TCO performance should be enhanced in the low thickness limit. Particularly, the In-based TCOs manifest explicit decrease of Φ as the film thickness decreases to values below a few hundreds of nanometers. Amorphous In-free CAO thin films indeed fill the gap in this thin-thickness limit, providing superior Φ ($\sim 10^{-2}$ Ω^{-1}) for the films as thin as 10 nm.

The exceptional homogeneity of the CAO thin films is the core feature for their TCO performance in the thin-thickness limit. In conventional crystalline In-based TCOs, the abrupt decrease of Φ is attributed to an increase in the grain boundary density as the thickness decreases.[20] On the other hand, the amorphous TCO thin films such as IZO and IZGO also show a degradation of the transport properties below 100 nm.[22] Substantial strain effect and the inhomogeneous defect distribution have been suggested as the cause of this degradation.[22] In contrast, the CAO thin films are highly uniform without any discernible thickness structural or chemical degradation, leading to a superior TCO figure of merit even for the thicknesses as low as ∼10 nm.

CONCLUSIONS

In summary, the amorphous CAO thin films are described and proposed as new In-free TCO materials of excellent performance. CAO thin films can be considered as one of the future TCO materials, because they are composed of earth-abundant elements and operate at the nanometer-thin thickness limit. In the thickness range investigated (10−50 nm), the amorphous CAO thin film shows a highly homogeneous structural quality, with good electrical conductivity and high transparency. Owing to its competitive performance as a TCO in the thin-thickness limit, the CAO thin film could lead the investigation of In-free TCO materials.

EXPERIMENTAL SECTION

Thin Film Fabrication and Structural Characterization. Atomically flat amorphous CAO thin films were grown on (001)-oriented single crystalline $SrTiO_3$ (STO) substrates, both single- and double-sided-polished, by using pulsed laser deposition (PLD) at 700 °C and oxygen partial pressure of 10^{-5} Torr. We used an excimer (KrF) laser with a wavelength of 248 nm (IPEX 864, Lightmachinery, Nepean, Canada), a low energy fluence of 0.76 J cm^{-2}, and a repetition rate of 8 Hz. We exploited the home-grown $CaAlO_{2.5}$ ceramic target. For the target, a 1:1 molar ratio of $CaCO_3$ (4 N) and Al_2O_3 (4 N) powders are mixed in an agate mortar and pressed into pellets of 20 mm in diameter. The pellets are subsequently fired at 1250 °C for 12 h. For the characterization of the amorphous structure, high-resolution X-ray diffraction (XRD) and transmission electron microscopy (JEM2100F, JEOL, KBSI) were employed. Atomic resolution STEM and EELS/EDS measurements were performed by Monochromated ARM200 (KBSI and GERI). The atomic force microscope (AFM) was used to reveal the atomically flat surface of the amorphous thin films. The X-ray reflectivity (XRR) measurements were employed to obtain the thickness values of amorphous CAO thin films, consistent with the TEM measurements.

Thin Film Chemical Composition. The chemical composition of the amorphous thin films was investigated using X-ray photoemission spectroscopy (XPS, Theta Probe, Thermo) at room temperature. A monochromated Al Kα ($h\nu$ = 1486.6 eV) was used as the source. The spot size of 400 μm and pass energy of 50.0 eV were employed for the measurements, with the steps of 0.1 eV. The peak positions were calibrated using the C 1*s* photoemission signal at 284.5 eV as reference. For the specific analysis of the spectra, we deconvoluted the peaks by using a mixed Gaussian−Lorentzian function.

Optical Properties Characterization. The transmittance spectra were measured using a commercial monochromatic spectrometer (Lambda 950, PerkinElmer). The measured spectra ranged from mid-infrared to UV (0.6−6.2 eV). An empty hole was used to define the reference transmittance. The both-side-polished STO substrates were employed for the transmittance measurements.

Transport Measurement. We used the van der Pauw geometry to simultaneously obtain the temperature dependent resistivity ρ and the carrier concentration *n*. Four Pt wires were attached on In electrodes at each corner of the square-shaped thin film to induce ohmic contact. For the Hall measurements, a current of 50 μA in a PPMS (Quantum Design) was applied under the temperatures ranging from 2 to 310 K.

Theoretical Interpretation. The first-principles molecular dynamics (MD) simulations and the electron structure calculations were performed using the Vienna *ab initio* simulation package (VASP).[45] The projector-augmented-wave pseudopotentials describe the electron−ion interactions.[46] The generalized gradient approximation (GGA) with the Perdew−Burke−Ernzerhof functional further characterizes the exchange-correlation energy between electrons.[47]

ASSOCIATED CONTENT

Supporting Information

The Supporting Information is available free of charge on the ACS Publications website at DOI: 10.1021/acs.chemmater.9b02399.

Supplementary figures, including details about XPS, DFT calculations, optical experiments, and TEM-EDS experiments (PDF)

AUTHOR INFORMATION

Corresponding Author

*(W.S.C.) E-mail: choiws@skku.edu.

ORCID

Hiroki Taniguchi: 0000-0002-1773-7856
Jae Hyuck Jang: 0000-0002-9133-3286
Woo Seok Choi: 0000-0002-2872-6191

Author Contributions

#(S.H.S. and K.T.K.) These authors contributed equally.

Author Contributions

The manuscript was written through contributions of all authors. All authors have given approval to the final version of the manuscript.

Notes

The authors declare no competing financial interest.

ACKNOWLEDGMENTS

This work was supported by the Basic Science Research Programs through the National Research Foundation of Korea (NRF-2019R1A2B5B02004546). Part of this study was performed using the facilities (optical spectroscopy) at the IBS Center for Correlated Electron Systems, Seoul National University. A Grant-in-Aid for Young Scientists (A) (No. 16H06115) and the MEXT Element Strategy Initiative Project to Form Core Research Center provided support. J.H.J. acknowledges the support by the New & Renewable Energy Core Technology Program of the Korea Institute of Energy Technology Evaluation and Planning (KETEP, Grant No. 20173010032080). T.P. acknowledges support by the Na-

DOI: 10.1021/acs.chemmater.9b02399
Chem. Mater. 2019, 31, 8019−8025

tional Research Foundation of Korea (Project no. 2012R1A3A2048816).

■ ABBREVIATIONS

TCO, transition metal oxide; ITO, indium tin oxide; CAO, Ca−Al−O; PLD, pulsed laser deposition; STO, $SrTiO_3$; XRR, X-ray reflectivity; AFM, atomic force microscopy; RMS, root-mean-square; TEM-EDS, transmission electron microscopy−electron dispersive spectroscopy; FFT, fast Fourier transformation; MD, molecular dynamics; XPS, X-ray photoelectron spectroscopy; STEM-EELS, scanning transmission electron microscopy−electron energy loss spectroscopy

■ REFERENCES

(1) Ellmer, K. Past Achievements and Future Challenges in the Development of Optically Transparent Electrodes. *Nat. Photonics* **2012**, *6*, 809.
(2) Wager, F. J. Transparent Electronics. *Science* **2003**, *300*, 1245.
(3) Guo, E.-J.; Guo, H.; Lu, H.; Jin, K.; He, M.; Yang, G. Structure and Characteristics of Ultrathin Indium Tin Oxide Films. *Appl. Phys. Lett.* **2011**, *98*, 011905.
(4) Taylor, M. P.; Readey, D. W.; van Hest, M. F. A. M.; Teplin, C. W.; Alleman, J. L.; Dabney, M. S.; Gedvilas, L. M.; Keyes, B. M; To, B.; Perkins, J. D.; Ginley, D. S. The Remarkable Thermal Stability of Amorphous In-Zn-O Transparent Conductors. *Adv. Funct. Mater.* **2008**, *18*, 3169.
(5) Edwards, P. P.; Porch, A.; Jones, M. O.; Morgan, D. V.; Perks, R. M. Basic Materials Physics of Transparent Conducting Oxides. *Dalton Trans* **2004**, 2995.
(6) Bender, M.; Seelig, W.; Daube, C.; Frankenberger, H.; Ocker, B.; Stollenwerk, J. Dependence of Film Composition and Thicknesses on Optical and Electrical Properties of ITO-metal-ITO Multilayers. *Thin Solid Films* **1998**, *326*, 67.
(7) Lee, J.-Y.; Connor, S. T.; Cui, Y.; Peumans, P. Solution-Processed Metal Nanowire Mesh Transparent Electrodes. *Nano Lett.* **2008**, *8*, 689.
(8) Kang, M.-G.; Guo, L. J. Nanoimprinted Semitransparent Metal Electrodes and Their Application in Organic Light-Emitting Diodes. *Adv. Mater.* **2007**, *19*, 1391.
(9) Iijima, S. Helical Microtubules of Graphitic Carbon. *Nature* **1991**, *354*, 56.
(10) Narushima, S.; Orita, M.; Hirano, M.; Hosono, H. Electronic Structure and Transport Properties in the Transparent Amorphous Oxide Semiconductor 2CdO GeO_2. *Phys. Rev. B: Condens. Matter Mater. Phys.* **2002**, *66*, 035203.
(11) Lewis, B. G.; Paine, D. C. Applications and Processing of Transparent Conducting Oxides. *MRS Bull.* **2000**, *25*, 22.
(12) Köstlin, H.; Jost, R.; Lems, W. Optical and Electrical Properties of Doped In_2O_3Films. *Phys. Status Solidi A* **1975**, *29*, 87.
(13) Yun, J. Ultrathin Metal Films for Transparent Electrodes of Flexible Optoelectronic Devices. *Adv. Funct. Mater.* **2017**, *27*, 1606641.
(14) Nomura, K.; Ohta, H.; Takagi, A.; Kamiya, T.; Hirano, M.; Hosono, H. Room-temperature Fabrication of Transparent Flexible Thin-film Transistors using Amorphous Oxide Semiconductors. *Nature* **2004**, *432*, 488.
(15) Hosono, H. Ionic Amorphous Oxide Semiconductors: Material Design, Carrier Transport, and Device Application. *J. Non-Cryst. Solids* **2006**, *352*, 851.
(16) Buchholz, D. B.; Ma, Q.; Alducin, D.; Ponce, A.; Jose-Yacaman, M.; Khanal, R.; Medvedeva, J. E.; Chang, R. P. H. The Structure and Properties of Amorphous Indium Oxide. *Chem. Mater.* **2014**, *26*, 5401.
(17) Mott, N. F.; Davis, E. A. *Electronic Processes in Non-crystalline Materials*; OUP: 2012.
(18) Cho, D.-Y.; Song, J.; Hwang, C. S.; Choi, W. S.; Noh, T. W.; Kim, J. Y.; Lee, H. G.; Park, B. G.; Cho, S. Y.; Oh, S. J.; Jeong, J. H.; Jeong, J. K.; Mo, Y.-G. Electronic Structure of Amorphous $InGaO_3(ZnO)_{0.5}$Thin Films. *Thin Solid Films* **2009**, *518*, 1079.
(19) Ginley, D. S.; Hosono, H.; Paine, D. C. *Handbook of Transparent Conductors*; Springer: 2010.
(20) Hao, L.; Diao, X.; Xu, H.; Gu, B.; Wang, T. Thickness Dependence of Structural, Electrical and Optical Properties of Indium Tin Oxide (ITO) Films Deposited on PET Substrates. *Appl. Surf. Sci.* **2008**, *254*, 3504.
(21) Li, X. D.; Chen, S.; Chen, T. P.; Liu, Y. Thickness Dependence of Optical Properties of Amorphous Indium Gallium Zinc Oxide Thin Films: Effects of Free-electrons and Quantum Confinement. *ECS Solid State Lett.* **2015**, *4*, P29−P32.
(22) Tsai, D.-C.; Chang, Z.-C.; Kuo, B.-H.; Wang, Y.-H.; Chen, E.-C.; Shieu, F.-S. Thickness Dependence of the Structural, Electrical, and Optical Properties of Amorphous Indium Zinc Oxide Thin Films. *J. Alloys Compd.* **2018**, *743*, 603.
(23) Lin, S.-S.; Huang, J.-L.; Lii, D.-F. The Effect of Thickness on the Properties of Ti-doped ZnOFilms by Simultaneous r.f. and d.c. Magnetron Sputtering. *Surf. Coat. Technol.* **2005**, *190*, 372.
(24) Zhang, L.; Zhou, Y.; Guo, L.; Zhao, W.; Barnes, A.; Zhang, H.-T.; Eaton, C.; Zheng, Y.; Brahlek, M.; Haneef, H. F.; Podraza, N. J.; Chan, M. H. W.; Gopalan, V.; Rabe, K. M.; Engel-Herbert, R. Correlated Metals as Transparent Conductors. *Nat. Mater.* **2016**, *15*, 204.
(25) Hu, L.; Wei, R.; Yan, J.; Wang, D.; Tang, X.; Luo, X.; Song, W.; Dai, J.; Zhu, X.; Zhang, C.; Sun, Y. $La_{2/3}Sr_{1/3}VO_3$Thin Films: ANew p-type Transparent Conducting Oxide with Very High Figure of Merit. *Adv. Electron. Mater.* **2018**, *4*, 1700476.
(26) Volintiru, I.; Creatore, M.; Van de Sanden, M. C. M. *In Situ*Spectroscopic Ellipsometry Growth Studies on the Al-doped ZnOFilms Deposited by Remote Plasma-Enhanced Metalorganic Chemical Vapor Deposition. *J. Appl. Phys.* **2008**, *103*, 033704.
(27) Steinhauser, J.; Faÿ, S.; Oliveira, N.; Vallat-Sauvain, E.; Ballif, C. Transition Between Grain Boundary and Intragrain Scattering Transport Mechanisms in Boron-doped Zinc Oxide Thin Films. *Appl. Phys. Lett.* **2007**, *90*, 142107.
(28) Singh, A. V.; Mehra, R. M.; Buthrath, N.; Wakahara, A.; Yoshida, A. Highly Conductive and Transparent Aluminum-deped Zinc Oxide Thin Films Prepared by Pulsed Laser Deposition in Oxygen Ambient. *J. Appl. Phys.* **2001**, *90*, 5661.
(29) Lee, S. A.; Jeong, H.; Woo, S.; Hwang, J.-Y.; Choi, S.-Y.; Kim, S.-D.; Choi, M.; Roh, S.; Yu, H.; Hwang, J.; Kim, S. W.; Choi, W. S. Phase Transitions via Selective Elemental Vacancy Engineering in Complex Oxide Thin Films. *Sci. Rep.* **2016**, *6*, 23649.
(30) Lee, H. N.; Ambrose Seo, S. S.; Choi, W. S.; Rouleau, C. M. Growth Control of Oxygen Stoichiometry in Homoepitaxial $SrTiO_3$Films by Pulsed Laser Epitaxy in High Vacuum. *Sci. Rep.* **2016**, *6*, 19941.
(31) Wong, F. J.; Baek, S.-H.; Chopdekar, R. V.; Mehta, V. V.; Jang, H.-W.; Eom, C.-B.; Suzuki, Y. Metallicity in $LaTiO_3$ Thin Films Induced by Lattice Deformation. *Phys. Rev. B* **2010**, *81*, No. 161101(R).
(32) Seo, S.S. A; Marton, Z.; Choi, W. S.; Hassink, G.W. J; Blank, D.H. A; Hwang, H. Y.; Noh, T. W.; Egami, T.; Lee, H. N. Multiple Conducting Carriers Generated in $LaAlO_3/SrTiO_3$Heterostructures. *Appl. Phys. Lett.* **2009**, *95*, 082107.
(33) Choi, W. S.; Rouleau, C. M.; Seo, S.S. A; Luo, Z.; Zhou, H.; Fister, T. T.; Eastman, J. A.; Fuoss, P. H.; Fong, D. D.; Tischler, J. Z.; Eres, G.; Chisholm, M. F.; Lee, H. N. Atomic Layer Engineering of Perovskite Oxides for Chemically Sharp Heterointerfaces. *Adv. Mater.* **2012**, *24*, 6423.
(34) Seo, I. W.; Lee, Y. S.; Lee, S. A.; Choi, W. S. Optical Investigation of Oxygen Defect States in $SrTiO_3$Epitaxial Thin Films. *Curr. Appl. Phys.* **2017**, *17*, 1148.
(35) Haacke, G. New Figure of Merit for Transparent Conductors. *J. Appl. Phys.* **1976**, *47*, 4086.
(36) Hymavathi, B.; Kumar, B. R.; Rao, T. S. Temperature Dependent Structural and Optical Properties of Nanostructured Cr

DOI: 10.1021/acs.chemmater.9b02399
Chem. Mater. 2019, 31, 8019−8025

Doped CdOThin Films Prepared by DC Reactive Magnetron Sputtering. *Procedia Mater. Sci.* **2014**, *6*, 1668.
(37) Moon, H.-J.; Gong, T.-K.; Kim, D.; Choi, D.-H.; Son, D.-I. Effect of a Cu Buffer Layer on the Structural, Optical, and Electrical Properties of IGZO/Cu Bi-layered Films. *Trans. Electr. Electron. Mater.* **2016**, *17*, 18−20.
(38) Wu, H.-C.; Chien, C.-H. High Performance InGaZnOThin Film Transistor withInGaZnOSource and Drain Electrodes. *Appl. Phys. Lett.* **2013**, *102*, 062103.
(39) Kim, J. H.; Lee, H.; Na, J.-Y.; Kim, S.-K.; Yoo, Y.-Z.; Seong, T.-Y. Optimization of Transmittance and Resistance of Indium Gallium zinc Oxide/Ag/indium Gallium Zinc Oxide Multilayer Electrodes for Photovoltaic Devices. *Curr. Appl. Phys.* **2015**, *15*, 452.
(40) Lee, H.-M.; Kang, S.-B.; Chung, K.-B.; Kim, H.-K. Transparent and Flexible Amorphous In-Si-O Films for Flexible Organic Solar Cells. *Appl. Phys. Lett.* **2013**, *102*, 021914.
(41) Kim, Y. C.; Lee, S. J.; Jung, H.; Park, B.-E.; Kim, H.; Lee, W.; Myoung, J.-M. Optimization and Device Application Potential of Oxide−metal−oxide Transparent Electrode Dtructure. *RSC Adv.* **2015**, *5*, 65094.
(42) Fraser, D. B.; Cook, H. D. Highly Conductive, Transparent Films of Sputtered $In_{2-x}Sn_xO_{3-y}$. *J. Electrochem. Soc.* **1972**, *119*, 1368.
(43) O'Connor, B.; Haughn, C.; An, K.-H.; Pipe, K. P.; Shtein, M. Transparent and Conductive Electrodes Based on Unpatterned, Thin Metal Films. *Appl. Phys. Lett.* **2008**, *93*, 223304.
(44) Martínez, L.; Ghosh, D. S.; Giurgola, S.; Vergani, P.; Pruneri, V. Stable Transparent Ni Electrodes. *Opt. Mater.* **2009**, *31*, 1115.
(45) Kresse, G.; Furthmüller, J. Efficient Iterative Schemes for Ab Initio Total-energy Calculations using a Plane-wave Basis Set. *Phys. Rev. B: Condens. Matter Mater. Phys.* **1996**, *54*, 11169.
(46) Blöchl, P. E. Projector Augmented-wave Method. *Phys. Rev. B: Condens. Matter Mater. Phys.* **1994**, *50*, 17953.
(47) Perdew, J. P.; Burke, K.; Ernzerhof, M. Generalized Gradient Approximation Made Simple. *Phys. Rev. Lett.* **1996**, *77*, 3865.

DOI: 10.1021/acs.chemmater.9b02399
Chem. Mater. 2019, 31, 8019−8025